ID: 1225

3D TIME DOMAIN FULL WAVEFORM INVERSION BASED ON MULTISCALE ADAPTED VARIABLE GRID METHOD CASE STUDY MAJUNGA BASIN EAST AFRICAN COAST

Mukiibi Ssewannyaga Ivan[1], Jian-Ping Huang[2], Zi-Ying Wang[3], Jidong Yang[4] Jin Keji[5]

ABSTRACT

The Full Waveform Inversion (FWI) method is a velocity building technique which exploits the richness of seismic waveforms to reconstruct high resolution velocity models. The multi-scale time-space strategy boosted the inversion accuracy of the structurally complex target and averted cycle skipping problems. Computational cost and storage requirement being the major drawbacks that inhibit the research and practical application of 3D full waveform inversion (FWI) parallel computing palatiform, Compute Unit Device Architecture (CUDA) was used to accelerate computation and adopted variable grids in the z-direction minimized the storage requirement. From the numerical results our adapted variable grid (VGFWI) not only increased the computation efficiency to almost twice the conventional technique at low frequency < 3Hzbut also gave more accurate results from the normalized root mean square error 4.18 and 4.5% noise free data respectively, thus enhances geologic structures both structural and stratigraphic features. From the dispersion relation, grid sizes adapted to local velocity with depth, which not only simulated wavefields with higher accuracy but also accelerated the calculation during the implementation of FWI. Our techniques successfully recovered the Marmousi and Majunga velocity structure amidst low signal to noise ratio data sets as compared to the conventional FWI technique. Numerous numerical tests coupled with quantitative analyses were carried out to verify the efficiency and accuracy of the technique on Majunga model, complex Marmousi and linear velocity model.

EXTENDED ABSTRACT

Introduction

Majunga basin is located in the northwestern quadrant of Madagascar, as up-to-date is the largest delineated salt basin in East Africa (Tari et.al., 2004, Coffin et.al., 1988). Majunga deep-water basin is characterized by a string of allochthonous salts, numerous salt-related play types mainly the simple four-way structural traps within the fold train of the toe-thrust zone at the outboard margin of the salt basin (Bally and Tari, 2004).

The exploration and development of deep-water sedimentary basins has become an important new field to increase the reserve and production of oil-gas resources around the world as easy to find hydrocarbon resources are nonexistent (He et al., 2006; Ma et. al., 2008, Pettingill and Weimer, 2001).

In a Geological context deep-water reservoir refers to systems that have been transported by gravity flow processes in a marine setting (Weimer, and Slatt 2004) Deep water is also defined as present-day sea depths in excess of 500 m (1640 ft) deep.

Globally the exploration level in the deep-water area is relatively low and the geological understanding is not clear.

Deep-water exploration in the Gulf of Mexico, Brazil, and west Africa is targeting and finding a large number of hydrocarbon pools in deep-water marine-sand systems. Only about 20% of these reservoirs have been developed to date (Mothi et al., 2012, Yannick, et.al., 2019). Full Waveform Inversion (FWI) method is a velocity building technique which exploits the richness of seismic waveforms to reconstruct high resolution velocity models.

Estimating an accurate velocity model is crucial step in both imaging and reservoir characterization. Targeting subtle structures including the numerous stratigraphic traps and minor faults requires very high-resolution technique. Conventional velocity model building techniques such as ray-based tomography and migration velocity analysis outputs inaccurate results (Yong, et al.,2018). In this paper we have studied 3D deep water basin full wave inversion using adapted variable grid tested on modified Marmousi model and deep offshore Majunga basin model generated from seismic salt related play interpreted section (Tari, et.al., 2004). Computational cost and storage requirement are the main obstacles that inhibit the research and practical application of full waveform inversion (FWI). In this study, we review and test Majunga generated model and modified Marmousi on conventional FWI techniques including the multiscale and in-depth analysis of proposed adapted full wave inversion (VGFWI) technique in comparison to the conventional FWI methods.

Theory and Methodology

Tarantola (1984) pioneered the research of FWI in the time domain. Crase et al. (1990), developed the time domain FWI technique. Pratt et al. (1998) extended FWI from the time domain to the frequency domain, based on the multi-scale strategy (Boonyasiriwat, et.al.,2009, Dessa, et.al., 2004).

In this paper the nonlinear conjugate gradient method is used in the determination of the descent direction. The hybrid scheme combining the Hestenes–Stiefel method and the Dai–Yuan method (Narayanan and Kaelo 2020) was used as the correction coefficient, modifying the descent direction and the Clayton and Enquist (1977) absorbing boundary conditions was adopted to absorb spurious reflections from the boundaries. We used the optimal finite difference method with accuracy of $O(\Delta t^2, \Delta x^8)$ as time-domain modeling operator.

In order to accelerate our 3D FWI algorithm and minimize computation cost we applied GPU parallelization techniques to boost efficiency in Cuda-C programming language. The average computation time required for an iteration using variable grid FWI was compared with the computing time to invert Majunga model using conventional FWI under the same conditions (Table 3). We implemented the GPU program on a workstation with NVIDIA Quadro P5000, which has 2560 processors, and 16 GB of GDDR5X memory.

Presence of thin and low velocity targets with high velocity contrasting beds the variable grid FWI technique is suitable technique to approximate velocities in these scenarios (Cai and Zhang, 2017). The following are the cons of using the regular scheme: regular coarse grids results into inaccurate solution of the wave equation; also it results into redundancy mainly in the deep high velocity zones resulting into a high computation cost and high demand on the

storage space (Wang and Schuster, 1996); When the near surface velocity is low or low-velocity targets exist in the deeper zone, such coarse-grid discretization will lead to inaccurate forward and backward wavefields due to dispersion phenomenon. On the other hand, if we use fixed fine grids throughout the model we get a good inversion results but at a huge expense of time and memory. Conventional variable grid technique refines and resolves specific zones within the model. The major drawback associated with this technique is the abrupt change from coarser grid to finer grids resulting into spurious reflections. Our method enables the grid size to increase gradually in the ***z*** direction and constant in ***x*** and ***y*** direction. The grid size change in the depth direction in a gradual manner since it is dependent on the velocity and depth (eqn.3) instead of an abrupt change in the transitional zone that usually amounts to several times the fine grid size. $\lambda_{min} = \frac{v_{min}}{f_{max}}$ (1)

Where λ_{min} is the minimum wavelength v_{min} minimum velocity and f_{max} maximum frequency. The ***z*** axis is modified based on the following equation $dz = \frac{v(z)}{nf_d}$ (2)

Where f_d denotes the dominant frequency and $v(z)$ is velocity variation with depth and n is the number of grid points per wavelength, which is set as ten in this work to ensure the wavefelds are adequately resampled. As a result, the number of velocity unknowns are reduced significantly, and inversion intends to resolve small-scale structures or the boundaries of large-scale structures. The approach is demonstrated by tests on synthetic velocity models i.e linear, deep water modified Marmousi and Majunga velocity model.

In our paper the algorithm coordinates only varies in the z direction and lateral changes are assumed constant. The first and second-order derivatives of z_{vg} with respect to the original physical coordinate variables z using a finite-difference method:

$$\frac{\partial z_{vg}}{\partial z} = \varphi'(z) \qquad (3)$$

Using inverse functions derivation procedures

$$\frac{\partial z}{\partial z_{vg}} = \frac{1}{\varphi'(z)} \qquad (4)$$

$$\frac{\partial^2 z}{\partial z_{vg}^2} = \partial\left(\frac{\frac{1}{\varphi'(z)}}{\partial z}\right)\frac{\partial z}{\partial z_{vg}} = \frac{\varphi''(z)}{[\varphi'(z)]^2}\frac{1}{\varphi'(z)} = -\frac{\varphi''(z)}{[\varphi'(z)]^3} \qquad (5)$$

From the conventional 3D acoustic wave equation in the time domain with regular grid ie,

$$\frac{1}{v^2(x)}\frac{\partial^2 u}{\partial t^2} = \left[\frac{\partial^2 u}{\partial x^2} + \frac{\partial^2 u}{\partial y^2} + \frac{\partial^2 u}{\partial z^2}\right] + f_s(t) \qquad (6)$$

Where v(x) is the velocity, $f_s(t)$ is the source signature, and u is the pressure field; x, y, z are the position in the regular-grid coordinates. We obtained the second derivative of the modified acoustic wave equation incorporating the variable grid variation property i.e

$$\frac{\partial \frac{\partial u}{\partial z_{vg}}}{\partial x}\frac{\partial x}{\partial z_{vg}} = \frac{\partial \frac{\partial u}{\partial z_{vg}}}{\partial x}\frac{\partial x}{\partial z_{vg}} + \frac{\partial \frac{\partial u}{\partial z_{vg}}}{\partial y}\frac{\partial y}{\partial z_{vg}} + \frac{\partial \frac{\partial u}{\partial z_{vg}}}{\partial z}\frac{\partial z}{\partial z_{vg}}$$

$$= \left[\frac{\partial^2 u}{\partial z^2}\frac{\partial z}{\partial z_{vg}} + \frac{\partial \frac{\partial z}{\partial z_{vg}}}{\partial z}\frac{\partial u}{\partial z}\right]\frac{\partial z}{\partial z_{vg}} \qquad (7)$$

$$= \frac{\partial^2 u}{\partial z^2}\left(\frac{1}{\varphi'(z)}\right)^2 - \frac{\partial u}{\partial z}\frac{\varphi''(z)}{[\varphi'(z)]^3}$$

In summary the modified formula is

$$\frac{1}{v^2(x)}\frac{\partial^2 u}{\partial t^2} = \left[\frac{\partial^2 u}{\partial x^2} + \frac{\partial^2 u}{\partial y^2} + \frac{\partial^2 u}{\partial z^2}\left(\frac{1}{\varphi'(z)}\right)^2 - \frac{\partial u}{\partial z}\frac{\varphi''(z)}{[\varphi'(z)]^3}\right] + f_s(t) \qquad (8)$$

Numerical tests

Example-1: Linear 3D velocity model

A cubic linearly varying velocity model (Fig.3) size grid size 300 uniformly spaced 10m with temporal step size dt=5ms was used to test the validity, accuracy and efficiency of our proposed technique. We used this model to demonstrate the accuracy and validity of our VGFWI algorithm by comparing the wavefields computed by our VGFWI wave equation to those computed by the convention FWI method. A single shot ejecting a ricker wavelet, dominant frequency of 10.0Hz was placed at the middle of the cube. Snapshots at different time intervals were recorded (table 1) maintaining the parameters for both VGFWI and FWI constant. Wave field snapshots middle-way along the x-axis for both schemes at 1.0s and corresponding vertical profile (Fig.4) at x=1.50 km were extracted. It can be observed that the wavefields are indistinguishable (Fig.4a &b). The difference between them is less than 1% thus differ slightly of the regular-grid wavefields which validates the accuracy and validity of our proposed scheme.

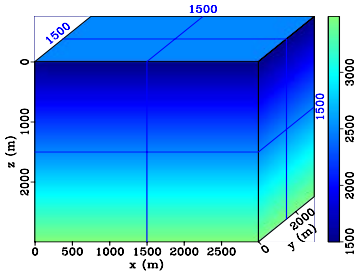

Figure: 3 ***Linear velocity model***

We extracted a vertical profile from snapshots (Fig.4c) above midway of the model (x=1.50km and y=1.50km) for the wavefield at 1.0s as observed VGFWI almost coincides with FWI profile this proves the validity of our new wave equation.

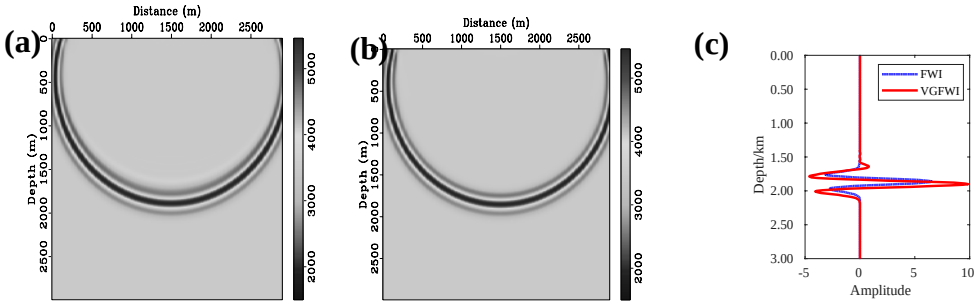

Figure 4: Snapshots at 1.0s 1500m in x and y calculated using ***a)*** VGFWI ***b)*** FWI equation and ***c)*** corresponding vertical profile at x=1.50km (record time=1.0s)

As it can be observed from (Table **1**), the time required to invert the linear velocity model in all cases using the conventional FWI equation is twice that of the proposed method at varying time records. This implies that VGFWI technique outperforms the conventional FWI in terms of computational efficiency.

Table 1: Elapsed time required to invert a sequence of backward wavefields at 0.50, 1.00, 1.50 and 2.00s time records. The wavefields are computed using the VGFWI and conventional FWI equations.

Wavefield snapshot /s	VGFWI (Time/s)	FWI (Time/s)
0.50	641.290	1214.860
1.00	675.182	1224.391
1.50	612.130	1239.670
2.00	654.087	1231.073

To evaluate the correctness of our final inverted model, we computed the normalized root mean square error (NRMS), given by

$$NRMS = \frac{1}{M^{max} - M^{min}} \sqrt{\frac{1}{M}\sum_{i-1}^{M}(m_i - m_i^{est})^2} \qquad (9)$$

Where, $\boldsymbol{M}$ denotes the number of parameters in the model vector, $\boldsymbol{m_i^{est}}$ final inverted model, m_i true model, M^{max} and M^{min} are the maximum and minimum values of the model parameters respectively. Quantitatively we computed the NRMS for final inverted with respect to true models for Majunga model in both noise-free and noisy data set (table 2) below.

Table 2 NMRS for VGFWI and FWI Majunga model noise free and noisy data

	VGFWI (NRMS%)	FWI (NRMS%)
Noise free	4.18	4.50
Noisy data	5.23	8.33

In either cases our technique gives a more accurate results proving its robustness to noise and improved inversion accurancy as compared to the conventional FWI technique. The robustness of VGFWI also is observable in the vertical profiles plot (Fig.10) below.

Example:2 Modified 3D Marmousi model

The truncated Marmousi 3D model consists of complicated geological structures with sharp boundaries and large velocity contrasting strata. It was modified by addition of 500m water layer to mimic deep-water basin. The truncated model consists of 124×269×51 grids with a spatial grid size of 20 m in all directions inversion results using VGFWI (Fig.5) for the different inversion stages (0-3Hz, 3-7Hz 7-12Hz and 12-15Hz) each 14 iterations are presented below. The marmousi structure in the final inversion scale is clearer Fig.5d below.

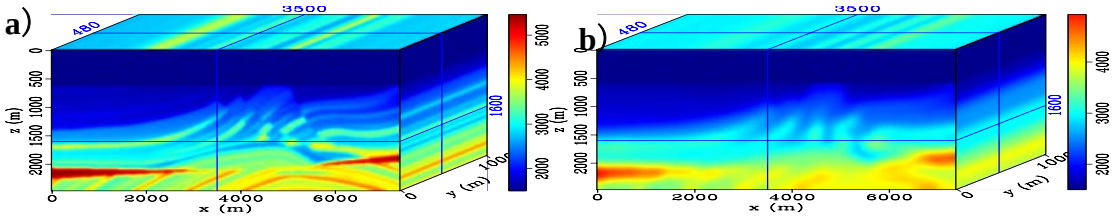

Figure 5 a) Modified Marmousi model b) Initial model

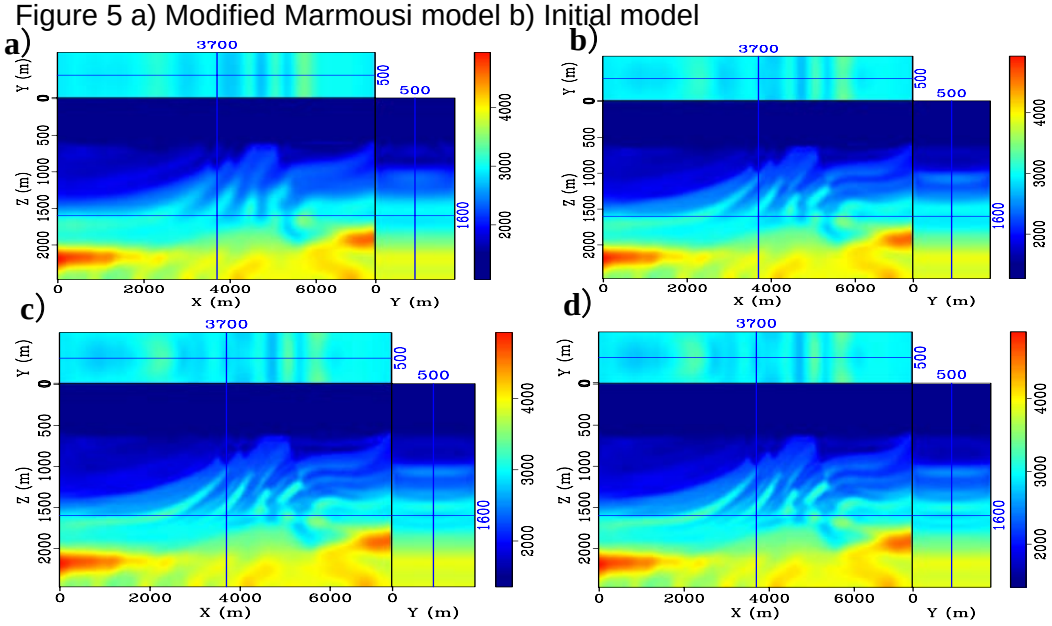

Figure 6: Multi scaled Inverted Model y=0.5km a) 0-3, b) 3-8, c) 8-12 and d) 12-15Hz

Example:3 Majunga Model

The majunga basin model was used because of the complex Geology commonly associated with both extensional and compressional regimes coupled with salt tectonics. The model was built using Tesseral 2D velocity model building software referring to generalized lithological map of Majuga basin (Bari and Tari, 2004) and extended into 3D space along the Y-direction. The model contains many reflectors, steep dips, vertical salt flanks, high angle normal faults and strong velocity variations in both the lateral and the vertical direction attributed to salt

diapirs. Conventional modeling and imaging techniques mainly fail to reveal these geological structures. Two independent tests on Majunga model regular grid (conventional FWI) and variable grid FWI using the multi scale approach to avert stacking in local minima were carried out. The survey configuration in both experiments were maintained. The model grid size for simulation 400×105×50 grid points, at spacing of 20m. The initial model for the inversion is obtained by smoothing the true velocity model using the multi-dimensional triangular smoothing (Gaussian function) as shown in (Fig.7b). A total of 190 shots (38 in x and 5 in y) at an interval of 100m were used in this experiment. A total of 9500 receivers were deployed at spacing of 10 and 20m in the 380 in ***x*** and 25 in ***y*** covering the entire grid. The data is recorded at a time increment of 0.8ms for a total of 2000 times. Ricker source wavelet with a peak frequency of 15Hz was used for synthetic generation. Bandpass filter between 0-3Hz, 3-7Hz and 7-15Hz was sequentially implemented for 13 iterations in each case. Slices of initial, true and inverted models at crossline location 4.0km inline location 0.5km and depth slice at 1.00km for both conventional FWI (Fig.8) and variable grid FWI (Fig.9) are presented below. With a Ricker wavelet of 3.0Hz dominant frequency, the velocity model is resampled to 56 grids in the depth direction from the original 108 grids in the z direction. The efficiency doubled the traditional FWI with fixed square grids. When we increased the dominant frequency to 7.0Hz the same trend as above was noted. However, at 7.0-15.0Hz inversion stage number of grids in z direction a slight increase in grid numbers compared to conventional method and reduction inefficiency though more updates are realized as shown in table 3 below. The method is suitable for real seismic data inversion because the computational cost is already good below 15Hz which is the standard for full wave form inversion as compared to the conventional technique and more accurate as observed in table 2 above. From the extracted depth profiles for the final FWI, VGFWI, initial and true velocity model (Fig.10) extracted at 0.5km and 4.0km in the ***x*** direction and 0.5Km in the ***y*** direction, the proposed method in (Fig.10a) provides more accurate values in the shallow and deeper parts of inverted velocity model than conventional FWI method. Generally deeper parts in both final inverted models show a noticeable velocity under-estimates from the true model (Fig.10) this is attributed to the relatively weak illumination, insufficient number of iterations etc.

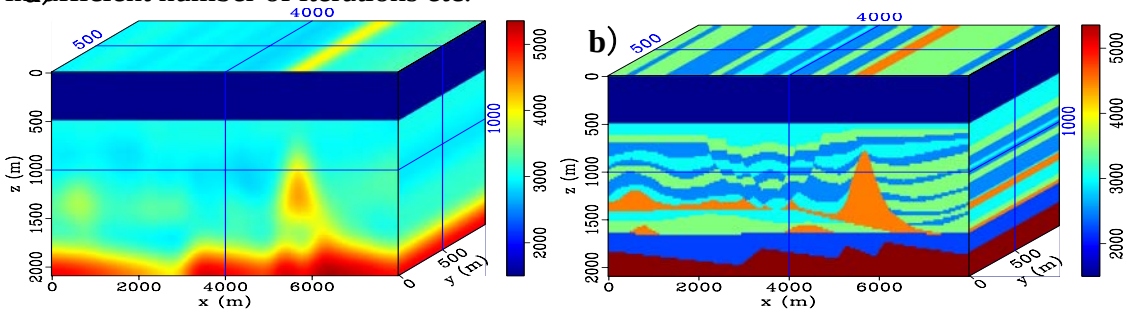

Figure 7: ***a)*** *Initial velocity model and* ***b)*** *True velocity model (horizontal time slice at 1.0Km, Inline 0.5Km and cross line positioned at 4.0km*

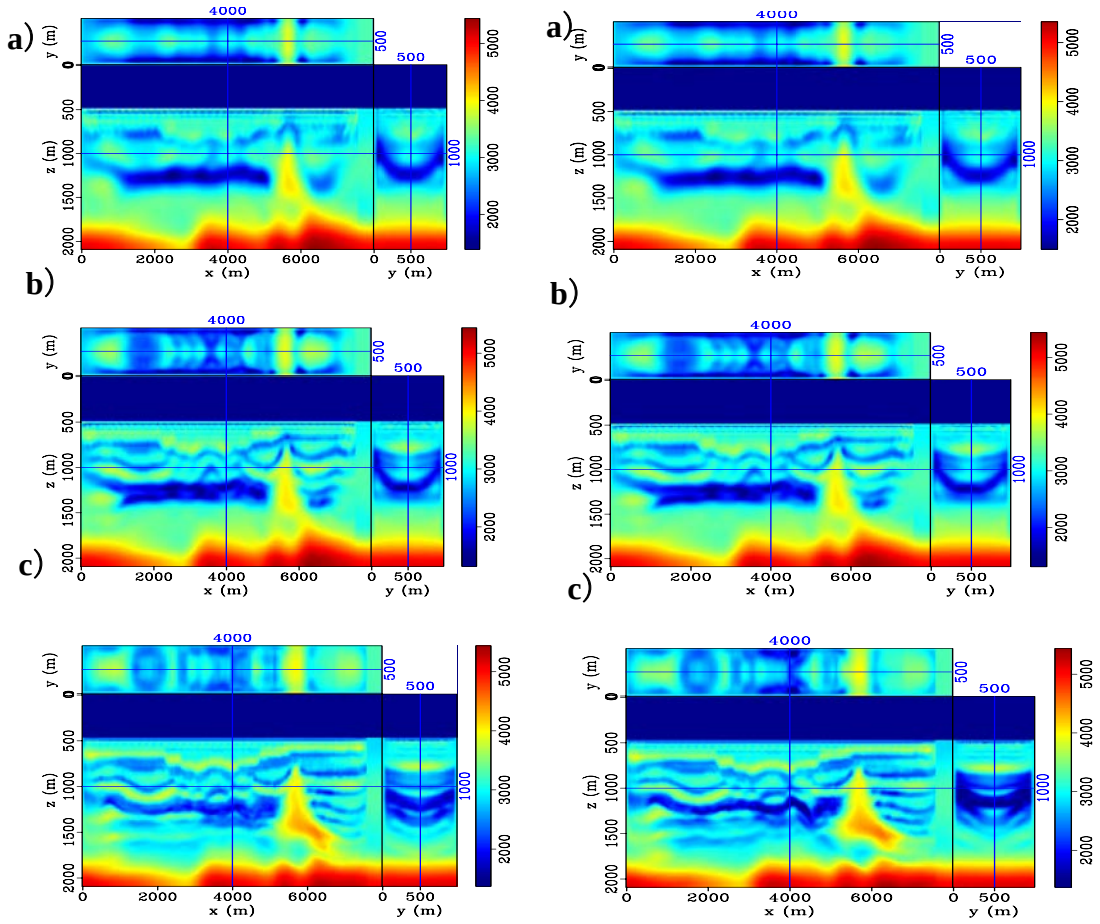

Figure 8: Adapted variable grid inverted velocity models between **a)** 0-3Hz, **b)** 3-7Hz and **c)** 7-15Hz for 13, 26 and 39 iterations respectively. (Horizontal slice z=1.0Km, Inline section at 0.5Km and crossline section at 4.0Km

Figure 9: Conventional inverted velocity models. **a)** 0-3Hz; **b)** 3-7Hz and **c)** 7-15Hz for 13, 26 and 39 iterations respectively.(Horizontal slice z=1.0Km, Inline section at 0.5Km and crossline section at 4.0Km

Table:3 Efficiency comparison between conventional multi-scale FWI and VGFWI

	Frequency range the wavelet	Grid number (nz)	Computing time for 1 iteration	Percentage of computing time	Efficiency improvement (%)
FWI	-	113	11961	-	-
Adapted variable FWI	0-3	60	7315	61.1	163
	3-7	99	11156	93.2	107
	7-15	151	15920	133	75

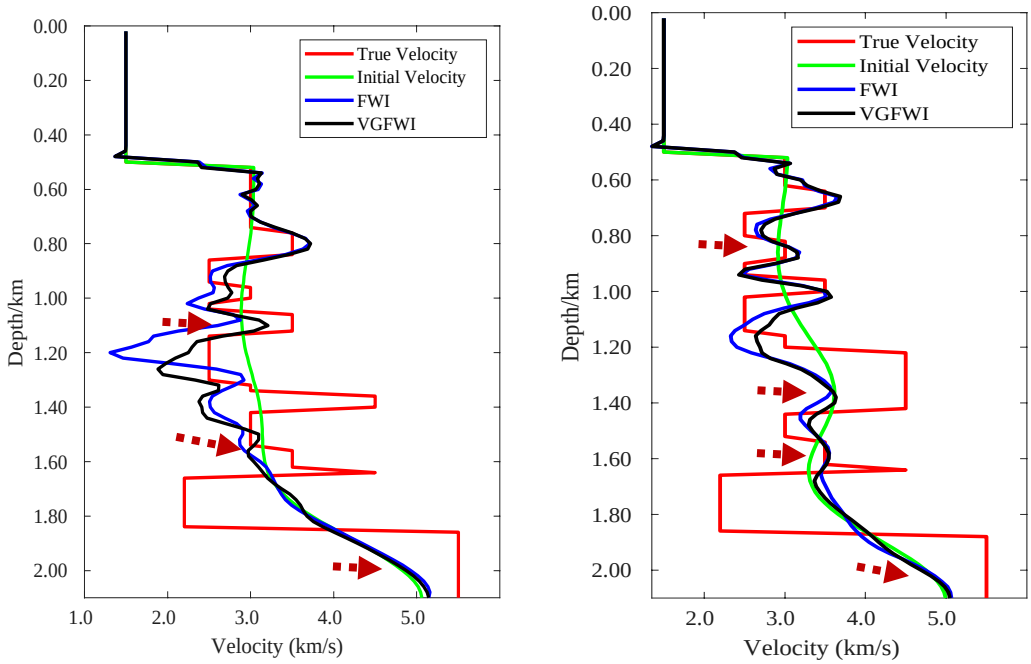

Figure 10: Comparison between vertical velocity profile of true, initial, conventional and VGFWI inverted models. ***a)*** Logs extracted at 2.0km and 0.5km and ***b)*** logs extracted at 4.0km and 0.5km in x and y. Red dotted arrows showing zones of enhanced resolution and where VGFWI approaches True velocity model in comparison with FWI.

Conclusion and recommendations

In this paper conventional/regular grid FWI and adaptive variable grid FWI using the Multi scale strategy approaches are tested on Marmousi, deep water Majunga basin models using acoustic 3D constant density wave equation accelerated on GPU. 3D Full wave inversion technology is inhibited by the expensive computational costs, storage and cycle skipping problems addressed by our technique. The computational efficiency with respect to the regular grid is increased to almost twice at a lower frequency range. Cycle skipping problems are successfully avoided by the multi- scale strategy approach of inverting the high wavelength structures using the lower frequencies and we gradually increase in the frequency bandwidth to recover the low wavelength structures. The multi scale strategy approach increases convergence chances to the global minima and minimizes the possibility of cycle skipping. From the numerical tests our cross sections, depth slices and profiles demonstrate that VGFWI is a cost-effective and quality-assured approach for 3D acoustic FWI in comparison with regular grid FWI. In future studies we intend to extend our adapted variable grid in both the X and Y direction to achieve more resolution and boost efficiency.

Acknowledgment

This research is supported by National Key R&D Program of China under contract number 2019YFC0605503C, the Major projects during the 14th Five-year Plan period under contract number 2021QNLM020001, the National Outstanding Youth Science Foundation under

contract number 41922028 and the Funds for Creative Research Groups of China under contract number 41821002. My sincere acknowledgement goes to Prof. Huang Jianping for his unwavering support.

References

1. Bally, A.W., Tari, G. C., 2004. Interpretation of seismic data in a regional context: developing frontier exploration opportunities: AAPG Winter Education Short Course, Houston, January 22, 2004
2. Bi, H. and Mothi S., 2012. Application of FWI to resolve gas cloud velocity anomaly in deep water Gulf of Mexico: 74th Conference and Exhibition, EAGE, Extended Abstracts, W014.
3. Boonyasiriwat, C., Valasek, P., Routh, P.,Weiping, C., Gerard, T.S. and Brian, M., 2009. An efficient multiscale for time-domain waveform tomography, Geophysics, 74, WCC59–68.
4. Cai A. and Zhang J., 2017. Variable Grid Traveltime Tomography for Near-surface Seismic Imaging American Geophysical Union, Fall Meeting 2017, abstract #NS33A-0026
5. Clayton, R. and Engquist, B., 1977. Absorbing boundary conditions for acoustic and elastic wave equations, Bulletin of the Seismological Society of America, 67, 1529–1540.
6. Coffin, M.F. and Rabinowitz, P.D., 1988, Evolution of the conjugate East African – Madagascar margins and the Western Somali Basin: Geological Society of America, Special Paper 226, 64 pp.
7. Crase, E., Pica, A., Noble, M., McDonald, J. and Tarantola, A. [1990] Robust elastic nonlinear waveform inversion: App
8. Dessa, J. X., Operto, S., Kodaira, S. and Nakanishi, A., Pascal, G., Virieux, J., Kaneda, Y., 2004. Multiscale seismic imaging of the eastern Nankai trough by full waveform inversion. Geophys. Res. Lett.31, doi: 10.1029/2004GL020453
9. He, J.X., Xia, B. and Shi, X.B., 2006. Prospect and progress for oil and gas in deep waters of the world and the potential and prospect foreground for oil and gas in deep waters of the South China Sea. Nature Gas Geoscience 17(6):747–752
10. Li, Q., Huang, J., Li, Z., Zhang, L. and Li, N., 2014. Forward modeling with adaptive variable-length spatial operators in pseudodepth domain, CPS/SEG Beijing 2014 International Geophysical Conference China University of Petroleum (East china).
11. Ma, L.W., Yu, S. and Tao,W.X., 2008. Analysis of deepwater sedimentary characteristics, southern Africa. Nat Gas Geosci 19(4):499–502pp
12. Mothi, S., Bi, H. and Yang, A., 2012. Benefits of FWI in Prestack Depth Imaging of Onshore Data. a Gulf Coast example. SEG Technical Program, Expanded Abstracts, 4205-4210
13. Mothi S., Schwarz K. and Zhu, H., 2013. Impact of full-azimuth and long-offset acquisition on Full Waveform Inversion in deep water Gulf of Mexico
14. Narayanan, S. and Kaelo, N. P., 2020. A Linear Hybridization of Dai-Yuan and Hestenes-Stiefel Conjugate Gradient Method for Unconstrained Optimization. Department of Mathematics, University of Botswana, Private Bag UB00704, Gaborone, Botswana, doi: 10.4208/nmtma.OA-2020-0056
15. Pettingill, H.S. and Weimer, P.,2001. Global deep-water exploration: Past, pesent and future frontiers, Global and Gulf of Mexico experience: GCS-SEPM Foundation,1-22pp.
16. Pratt, R.G., Shin, C. and Hicks, G.J., 1998. Gauss-Newton and full Newton methods in frequency-space seismic waveform inversion, Geophysical Journal International, 133, 341–362.
17. Tari, G., Coterill, K., Molnar, J., Valasek, D., Walters, G. and Alvarez, Y., 2004. Salt Tectonics and Sedimentation in the Offshore Majunga Basin, Madagascar. Vanco Energy Company pp 1-27pp.
18. Tarantola, A., 1984. Inversion of seismic reflection data in the acoustic approximation. Geophysics 49, 1259–1266.
19. Wang, K., Deng, B., Zhang, Z., Hu, L. and Huang, Y., 2015.Top of salt impact on full waveform inversion sediment velocity update: 85th Annual International Meeting, SEG, Expanded Abstracts, 1072–1077PP.
20. Wang Z., Huang J., Liu D., Li Z., Yong P. and Yang Z., 2018. 3D variable-grid full-waveform inversion on GPU. Petroleum Science (2019) 16:1001–1014, https://doi.org/10.1007/s12182-019-00368-2
21. Wang, Y. and Schuster, G.T., 1996. Finite-difference variable grid scheme for acoustic and elastic wave equation modeling Dept. of Geology.
22. Weimer, P. and Slatt, R. M., 2004. Petroleum systems of deep-water settings: SEG/EAGE (Society of Exploration Geophysicists/European Association of Geoscientists and Engineers) Distinguished Instructor Series 7, 465
23. Yannick, C., Carlos, C. and Shihong, C., 2019. Full-waveform inversion for imaging and geologic interpretation: A deepwater Gulf of Mexico case study. SEG and AAPG, Vol. 7, No. 2 p. 1–11, 18 FIGS. http://dx.doi.org/10.1190/INT-2018-0163.1.
24. Yong, P., Liao, W., Huang, J., Li, Z. and Lin, Y., 2018. Misfit function for full waveform inversion based on the Wasserstein metric with dynamic formulation [J]. Journal of Computational Physics, 2019, 399: 108911.

Hosted by Ministry of Oil

Supported by nogaholding

Chaired by aramco

Co-chaired by ADNOC eni

Conference Organisers AAPG EAGE SEG SPE

Event Organisers informamarkets